JOURNAL OF GEOPHYSICAL RESEARCH, VOL. 115, D06208, doi:10.1029/2009JD012304, 2010

A modified method for inferring upper troposphere cloud top height using the GOES 12 imager 10.7 and 13.3 μm data

Fu-Lung Chang,[1,2] Patrick Minnis,[3] Bing Lin,[3] Mandana M. Khaiyer,[4] Rabindra Palikonda,[4] and Douglas A. Spangenberg[4]

Received 23 April 2009; revised 1 October 2009; accepted 23 November 2009; published 30 March 2010.

[1] Passive satellite retrievals using conventional CO_2 absorption techniques tend to systematically underestimate the upper transmissive cloud top heights (CTHs). These techniques are based on single-layer assumptions that the upper cloud occupies a geometrically thin layer above a cloud-free surface. This study presents a new modified CO_2 absorption technique (MCO2AT) to improve the inference of transmissive CTHs in the upper troposphere above 600 hPa. The MCO2AT employs an iterative algorithm that starts with a single-layer CO_2 absorption technique (SCO2AT) followed by an iterative procedure to retrieve an enhanced upper CTH based on inferred effective background radiances. Both techniques are applied to the 10.7 and 13.3 μm channel data of the Twelfth Geostationary Operational Environmental Satellite (GOES 12) imager and their retrievals of upper tropospheric CTHs are compared with two active sensing products: the ground-based Active Remotely Sensed Cloud Location (ARSCL) products from the Atmospheric Radiation Measurement Program (ARM) Southern Great Plains (SGP) site and the satellite-based Cloud Aerosol Lidar With Orthogonal Polarization (CALIOP) products. On average, the CTHs from MCO2AT and SCO2AT are lower than those from both of the active sensors by ~1 and 2.4 km, respectively, possibly due to the different sensitivities and spatial resolutions between passive and active sensors. Preliminary validation of the new modified method is encouraging, especially the improvements for upper transmissive clouds in geometrically thick and/or multilayered cloud situations. The development of the modified method is particularly useful for sensors like the GOES 12, Meteosat-9, and others, which carry only one CO_2 absorption channel at ~13.3 μm.

Citation: Chang, F.-L., P. Minnis, B. Lin, M. M. Khaiyer, R. Palikonda, and D. A. Spangenberg (2010), A modified method for inferring upper troposphere cloud top height using the GOES 12 imager 10.7 and 13.3 μm data, *J. Geophys. Res.*, *115*, D06208, doi:10.1029/2009JD012304.

1. Introduction

[2] To infer upper troposphere cloud top height (CTH), passive meteorological satellites usually employ a window technique that is based on analyses of radiances measured in the visible and infrared (IR) window channels [e.g., *Rossow and Schiffer*, 1991; *Minnis et al.*, 1993, also CERES Edition-2 cloud property retrievals using TRMM VIRS and Terra and Aqua MODIS data, Part I: Algorithms; Part II: Examples of average results and comparisons with other data, submitted to *IEEE Transactions on Geoscience and Remote Sensing*, 2010] or on a CO_2-slicing technique that is based on analyses of the IR radiances obtained in various CO_2 absorption spectral bands [e.g., *Chahine*, 1974; *McCleese and Wilson*, 1976; *Smith and Platt*, 1978; *Smith and Frey*, 1990; *Menzel et al.*, 1983, 1992]. Standard window techniques tend to underestimate the occurrence of highly transmissive cirrus clouds [*Rossow*, 1989; *Wylie and Menzel*, 1989; *Jin et al.*, 1996]. Often, these underestimated cirrus clouds can be detected using the CO_2-slicing technique to infer a cloud top pressure (CTP) and, hence, the CTH. However, past validation studies have reported that the CTHs inferred by the CO_2-slicing techniques were systematically underestimated by a range of ~1 km to more than 3 km, depending on the transmissive nature of upper clouds [*Wylie and Menzel*, 1989; *Frey et al.*, 1999; *Schreiner et al.*, 2001; *Hawkinson et al.*, 2005; *Holz et al.*, 2006; *Bedka et al.*, 2007; *Smith et al.*, 2008]. Other validation studies using the window techniques for deep convection and optically thick ice clouds have reported ~1–2 km underestimation of CTHs [*Sherwood et al.*, 2004; *Minnis et al.*, 2008].

[3] Window techniques have typically been used to analyze the high-resolution (~4 km) imager data on the Geo-

[1]National Institute of Aerospace, Hampton, Virginia, USA.
[2]Now at Science Systems and Applications, Inc., Hampton, Virginia, USA.
[3]NASA Langley Research Center, Hampton, Virginia, USA.
[4]Science Systems and Applications Inc., Hampton, Virginia, USA.

0148-0227/10/2009JD012304

stationary Operational Environmental Satellite (GOES) series, GOES 8 through 11 [e.g., *Smith et al.,* 2008], which measure radiances at five wavelengths, nominally 0.65, 3.9, 6.7, 10.7 and 12 μm [*Menzel and Purdom*, 1994]. However, beginning with GOES 12, the GOES-I imager series have replaced the 12 μm channel with a new 13.3 μm channel to improve the cloud products derived from the GOES-I imagers [*Schmit et al.*, 2001]. Techniques are needed to efficiently exploit this new channel complement for retrievals of cloud properties.

[4] To that end, this study explores a new modified CO_2 absorption technique (MCO2AT) that uses the GOES 12 imager 10.7 and 13.3 μm channel data for improving the inference of upper troposphere CTHs. Since the performance of a two-channel CO_2 absorption technique depends on the channels used, different channel selections can thus result in different CTH solutions [*Wielicki and Coakley*, 1981; *Eyre and Menzel*, 1989]. Using lower-wavelength sounding channels, which have the least atmospheric absorption, permits a CTH retrieval for the majority of clouds throughout the troposphere. Higher-wavelength sounding channels, which are more absorbing, limit the detection to high-level clouds only due to increased atmospheric opacity and reduced signal-to-noise ratios. However, it was also noted that CTH retrieval skill depends on the accuracy of the specified background radiances. For the case of single-layer clouds, the background radiances are assumed to be the clear-sky radiances. For complex multilayer cases (e.g., cirrus over stratus), the background radiances for the upper-level CTH retrieval are no longer the clear-sky radiances but rather the radiances emitted from the lower-level cloud and intervening atmosphere. While use of the clear-sky radiances may be appropriate for single-layer cases, it is usually not appropriate for multilayer cases and often leads to underestimates in upper-level CTHs [*Chang and Li*, 2005]. Thus, accurately characterizing the proper background radiances is particularly important for improving upper transmissive CTH retrievals.

[5] The primary objective of the MCO2AT is to improve the retrievals of upper troposphere transmissive CTH for both multilayer clouds and for geometrically thick, but optically thin clouds. The traditional single-layer CO_2 absorption technique (SCO2AT) often assumes that the cloud occupies a single layer in the field of view (FOV) of the satellite instrument and the single-layer cloud occupies infinitesimal or zero thickness by neglecting the cloud geometric thickness effect. *Chang and Li* [2005] compared the single-layered and multilayered cloud properties derived from the Moderate Resolution Imaging Spectroradiometer (MODIS) data and reported that the CO_2-slicing CTPs for multilayer clouds were likely overestimated by 40 hPa on a global scale due to single-layer assumptions. *Holz et al.* [2006] used the hyperspectral Scanning High-Resolution Interferometer Sounder (S-HIS) data and reported that for geometrically thick but optically thin clouds, the CO_2-slicing CTHs were underestimated by more than 3 km. The MCO2AT is thus developed to infer the effective background radiances to replace the clear-sky radiances. Use of the background radiance should reduce the underestimation of upper cirrus CTH caused by any underlying lower cloud and/or to reduce the underestimation of top heights for geometrically thick, tenuous clouds. It could also provide a better estimate of the true clear-sky radiances when they are based on uncertain estimates of surface temperature.

[6] The method is initially tested using data from GOES 12. To evaluate the retrievals of upper tropospheric CTHs by both the MCO2AT and SCO2AT, GOES 12 half-hourly scanning data are matched with two active remote sensing products: the ground-based Active Remotely Sensed Cloud Location (ARSCL) products [*Clothiaux et al.*, 2000] from the Atmospheric Radiation Measurement (ARM) Program [*Ackerman and Stokes*, 2003] Southern Great Plains site and the space-based Cloud-Aerosol Lidar and Infrared Pathfinder Satellite Observation (CALIPSO) cloud vertical mask products measured by the Cloud Aerosol Lidar with Orthogonal Polarization (CALIOP) [*Winker et al.*, 2007].

[7] Section 2 describes the data sets used herein, and section 3 presents the iterative algorithm of the MCO2AT that starts with the SCO2AT CTH retrieval. Section 4 presents the results obtained with the MCO2AT and the SCO2AT and their comparisons with the results obtained from the ARSCL and the CALIOP. Section 5 gives the concluding remarks.

2. Data

2.1. GOES 12 and ARSCL Data

[8] To examine the performance of the MCO2AT-retrieved CTHs, this study uses the half-hourly GOES 12 imagery taken about 15 and 45 min after the UTC hour. The ARSCL-inferred CTHs are compared with retrievals using GOES 12 imagery data taken during May 2005. During this month, the ARM SGP Cloud and Radiation Test Bed (CART) in Lamont, Oklahoma, was frequently cloudy, having various cloud types almost every day. The half-hourly GOES 12 data for the SGP domain were taken from the NASA Langley ARM imagery and cloud product archives [*Ayers et al.*, 2006] (see http://www-angler.larc.nasa.gov/). Those images have a convolved 4 km × 3.2 km spatial resolution at nadir. The original scanning resolution is about 4 km × 2.3 km (north-south direction × east-west direction) for the 10.7 μm channel and about 8 km × 2.3 km (north-south × east-west) for the 13.3 μm channel. At the ARM SGP CART site (36.6°N, 97.5°W), the GOES 12 imager has an oblique satellite viewing zenith angle of ~48° that degrades its spatial resolution by a factor of ~1.5 compared to the nadir view.

[9] The ARSCL provides a time series of cloud top and cloud base heights for single-layer or multilayer clouds observed at the ARM SGP CART site with an up-looking spatial resolution of ~45 m and a temporal sampling rate at 10 s intervals [*Clothiaux et al.*, 2000]. The ARSCL algorithm combines the ground-based active remote sensing measurements from both a millimeter-wavelength cloud radar (MMCR) and a micropulse lidar (MPL) to estimate the locations of cloud top and cloud base heights. Since the ARSCL produces a much finer resolution time series data than the GOES 12 imager, the ARSCL uppermost CTHs are averaged over a 3 min period centered at the time when the imager scanned across the CART site. On the other hand, since the GOES 12 has an oblique view at the CART site, the imager pixels obtained within a 15 km × 15 km area centered at the CART site are analyzed to determine the number of pixels having upper troposphere CTHs retrieved by the MCO2AT and SCO2AT. The number of CTH-retrieved

pixels serves as a spatial uniformity check when comparing the CTH differences between the two data sets.

2.2. GOES 12 and CALIOP Data

[10] Comparisons of the CALIOP- and GOES 12-inferred CTHs are performed using data from April 2007. Because of CALIPSO's orbit, CALIOP data are only available around 1330 LT at different locations each day. The CALIOP is a nadir-pointing instrument that samples every 330 m with a spatial resolution (footprint) of ~70 m. It uses 532 and 1064 nm lidars to profile clouds and aerosols [*Winker et al.*, 2007], providing CTHs, for each observed layer until the beam is attenuated.

[11] The CALIOP and GOES data are matched first based on the collocation of the two satellite data where the time difference between the observations is no more than ±10 min. Since the GOES 12 data have various satellite viewing zenith angles, for every matched data pair, a 3 × 3 pixel array from GOES 12 is used for analyses of the MCO2AT- and SCO2AT-retrieved CTHs. The CALIOP data falling within the 3 × 3 pixel array and within ±10 min of the observation time difference are used in the comparison. The sensitivities of the GOES-CALIOP CTH differences to observation time difference, the imager viewing zenith angle, and the number of GOES 12 imager pixels with valid MCO2AT and SCO2AT retrievals are examined in section 4.2.

3. Techniques

3.1. Single-Layer CO_2 Absorption Technique

[12] Since conventional CO_2 absorption techniques are based on a single-layer cloud assumption, we briefly describe the SCO2AT that utilizes the radiance pair obtained by the GOES 12 imager at the 10.7 μm and 13.3 μm channels. For simplicity, hereafter we use the superscript 11 to denote the 10.7 μm channel and superscript 13 to denote the 13.3 μm channel.

[13] Let us begin by considering the clear-sky radiances R^{11}_{clr} and R^{13}_{clr} for the two channels, which are given by

$$R^{11}_{clr}(T_g|P_g) = B^{11}(T_g)\xi^{11}(P_g) + \int_{P_g}^{0} B^{11}(T(P))\frac{d\xi^{11}(P)}{d\ln P}d\ln P \tag{1}$$

$$R^{13}_{clr}(T_g|P_g) = B^{13}(T_g)\xi^{13}(P_g) + \int_{P_g}^{0} B^{13}(T(P))\frac{d\xi^{13}(P)}{d\ln P}d\ln P, \tag{2}$$

where T_g and P_g denote the ground surface temperature and pressure, B^{11} and B^{13} denote the Planck function, and $\xi^{11}(P)$ and $\xi^{13}(P)$ denote the transmittance between TOA ($P = 0$) and pressure-level P for the two channels. In (1) and (2), the surface emissivity is assumed to be unity. Similarly, the opaque overcast radiances R^{11}_{ovc} and R^{13}_{ovc} for the two channels are given by

$$R^{11}_{ovc}(T_c|P_c) = B^{11}(T_c)\xi^{11}(P_c) + \int_{P_c}^{0} B^{11}(T(P))\frac{d\xi^{11}(P)}{d\ln P}d\ln P \tag{3}$$

$$R^{13}_{ovc}(T_c|P_c) = B^{13}(T_c)\xi^{13}(P_c) + \int_{P_c}^{0} B^{13}(T(P))\frac{d\xi^{13}(P)}{d\ln P}d\ln P, \tag{4}$$

where T_c and P_c denote the cloud top temperature and pressure.

[14] In the two IR channels, cloud reflectivity is often negligible and, thus, cloud transmissivity t_c can be related to cloud emissivity e_c by $t_c = 1 - e_c$. As such, the satellite-observed radiances R^{11}_{obs} and R^{13}_{obs} for a semitransparent cloudy pixel are given by

$$R^{11}_{obs} = \varepsilon^{11}_c R^{11}_{ovc}(T_c|P_c) + (1-\varepsilon^{11}_c)R^{11}_{clr}(T_g|P_g) \tag{5}$$

$$R^{13}_{obs} = \varepsilon^{13}_c R^{13}_{ovc}(T_c|P_c) + (1-\varepsilon^{13}_c)R^{13}_{clr}(T_g|P_g), \tag{6}$$

where $\varepsilon_c = e_c A_c$ denotes an effective cloud emissivity with e_c being the cloud emissivity and A_c being the cloud cover fraction of the imager pixel. In (5) and (6), $R_{obs} = R_{ovc}$, if $\varepsilon_c = 1$ or $R_{obs} = R_{clr}$, if $\varepsilon_c = 0$.

[15] We can manipulate (5) and (6) to derive the ratios of the two channels for the cloud radiative effects to yield

$$\frac{R^{13}_{obs} - R^{13}_{clr}(T_g|P_g)}{R^{11}_{obs} - R^{11}_{clr}(T_g|P_g)} = \frac{\varepsilon^{13}_c(R^{13}_{ovc}(T_c|P_c) - R^{13}_{clr}(T_g|P_g))}{\varepsilon^{11}_c(R^{11}_{ovc}(T_c|P_c) - R^{11}_{clr}(T_g|P_g))}. \tag{7}$$

The ratios in (7) represent the cloud radiative effects where the left-hand side represents satellite observations and the right-hand side can be estimated through radiative transfer calculations for specified T_c and P_c. For an observed pair of R^{11}_{obs} and R^{13}_{obs}, the solution $T_c|P_c$ is obtained by minimizing the differences between the two sides of (7) with the specified $T_g|P_g$. In conventional CO_2 absorption approaches, the differences in IR spectral emissivities are often assumed negligible, i.e., $\varepsilon^{11}_c \approx \varepsilon^{13}_c$.

[16] The input atmospheric profiles of temperature, pressure, height and humidity for calculating the clear-sky and overcast radiances in (1)–(4) are taken from the NOAA National Centers for Environmental Prediction (NCEP) 1-hourly Rapid Update Cycle (RUC) model analysis data set with a 40 km spatial resolution [*Benjamin et al.*, 2004a, 2004b]. The hourly RUC data set covers a large portion of North America including the Contiguous United States (CONUS). The widely used MODTRAN4 radiative transfer code [*Berk et al.*, 1999] is used for simulations of the spectral radiances.

3.2. Modified CO_2 Absorption Technique

[17] The MCO2AT is a modified version of the SCO2AT. As the SCO2AT assumes clouds being single-layered with a clear-sky background, the MCO2AT is proposed to use inferred effective background radiances to replace the clear-sky radiances. In an idealized two-layer cloud situation, the effective background radiances represent the blackbody lower-cloud radiances. In reality, the effective background radiances are often a mixture of clear-sky radiances and/or lower-cloud radiances in single-layer and/or multilayer cloud situations.

[18] In essence, the MCO2AT determines the effective background temperature T_{ebg} and effective background

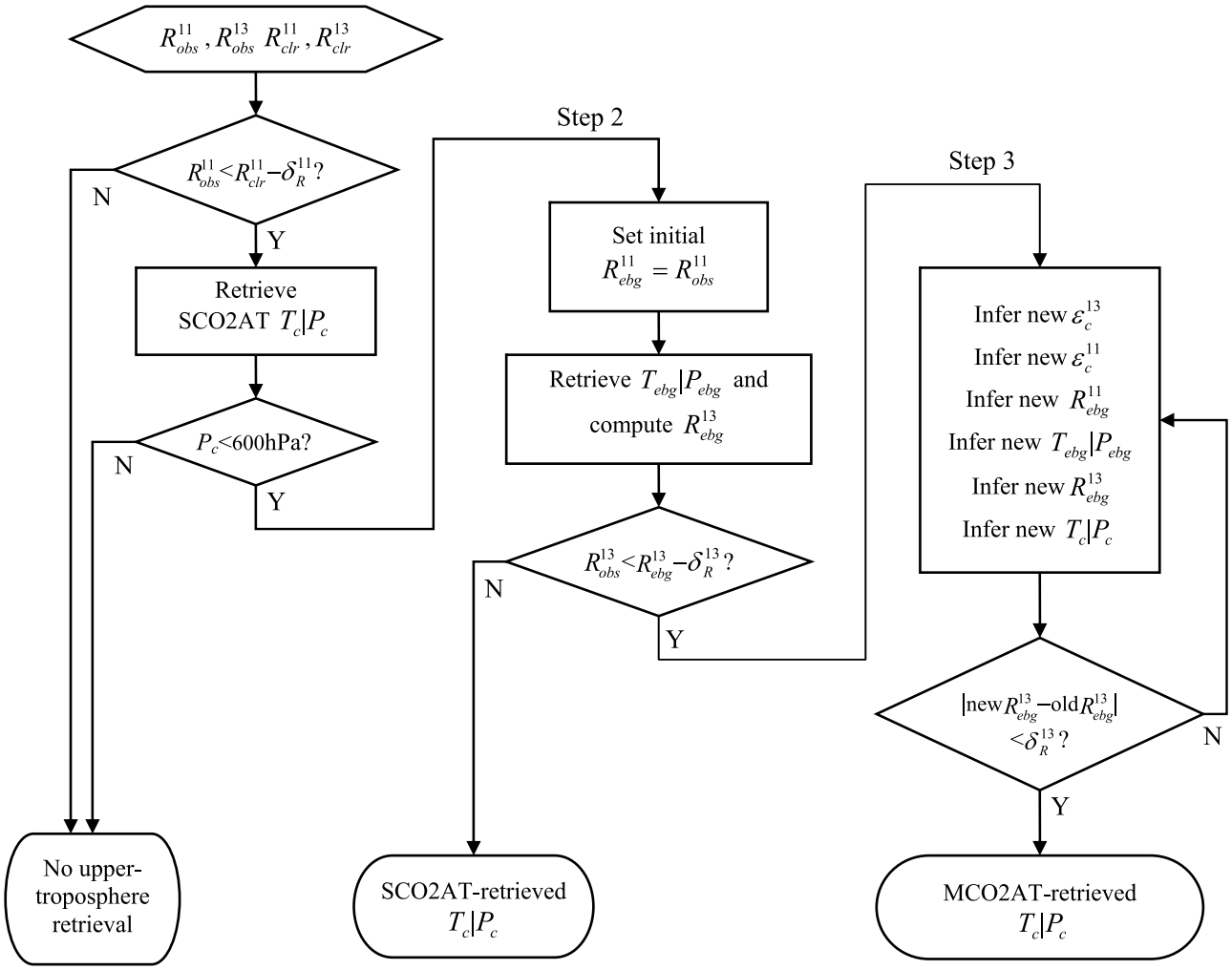

Figure 1. Schematic diagram for illustrating the SCO2AT and MCO2AT algorithms.

pressure P_{ebg} in contrast to the T_g and P_g in the SCO2AT. As such, equation (7) is modified in the MCO2AT and given by

$$\frac{R^{13}_{obs} - R^{13}_{ebg}(T_{ebg}|P_{ebg})}{R^{11}_{obs} - R^{11}_{ebg}(T_{ebg}|P_{ebg})} = \frac{\varepsilon^{13}_c(R^{13}_{ovc}(T_c|P_c) - R^{13}_{ebg}(T_{ebg}|P_{ebg}))}{\varepsilon^{11}_c(R^{11}_{ovc}(T_c|P_c) - R^{11}_{ebg}(T_{ebg}|P_{ebg}))}, \tag{8}$$

where

$$R^{11}_{ebg}(T_{ebg}|P_{ebg}) = B^{11}(T_{ebg})\xi^{11}(P_{ebg}) + \int_{P_{ebg}}^{0} B^{11}(T(P))\frac{d\xi^{11}(P)}{d\ln P} d\ln P \tag{9}$$

$$R^{13}_{ebg}(T_{ebg}|P_{ebg}) = B^{13}(T_{ebg})\xi^{13}(P_{ebg}) + \int_{P_{ebg}}^{0} B^{13}(T(P))\frac{d\xi^{13}(P)}{d\ln P} d\ln P. \tag{10}$$

We also relate ε^{11}_c and ε^{13}_c through

$$\frac{\varepsilon^{13}_c}{\varepsilon^{11}_c} = \frac{1 - \exp(-\tau^{13}_c/\mu)}{1 - \exp(-\tau^{11}_c/\mu)} \tag{11}$$

$$\frac{\tau^{13}_c}{\tau^{11}_c} = \frac{\sigma^{13}_{ext}}{\sigma^{11}_{ext}}, \tag{12}$$

where τ^{11}_c and τ^{13}_c denote the corresponding spectral cloud optical depths, σ^{11}_{ext} and σ^{13}_{ext} denote the corresponding spectral extinction coefficients, and μ denotes the cosine of satellite viewing zenith angle. Here we adopt $\sigma^{11}_{ext}/\sigma^{13}_{ext} = 1.12$ for an approximate range of $\sigma^{11}_{ext}/\sigma^{13}_{ext} = 1.02$–$1.25$ for various ice crystal size distributions [e.g., *Yang et al.*, 2001].

[19] To solve for $T_c|P_c$ using (8), the MCO2AT needs to determine $T_{ebg}|P_{ebg}$ using an iterative retrieval algorithm. The algorithm as presented in Figure 1 consists of three main steps. The first step is to apply the SCO2AT if the satellite-observed R^{11}_{obs} is less than $R^{11}_{clr} - \delta^{11}_R$. Here, a threshold $\delta^{11}_R = 0.5$ Wm^{-2}sr$^{-1}\mu$m^{-1} is used to account for the

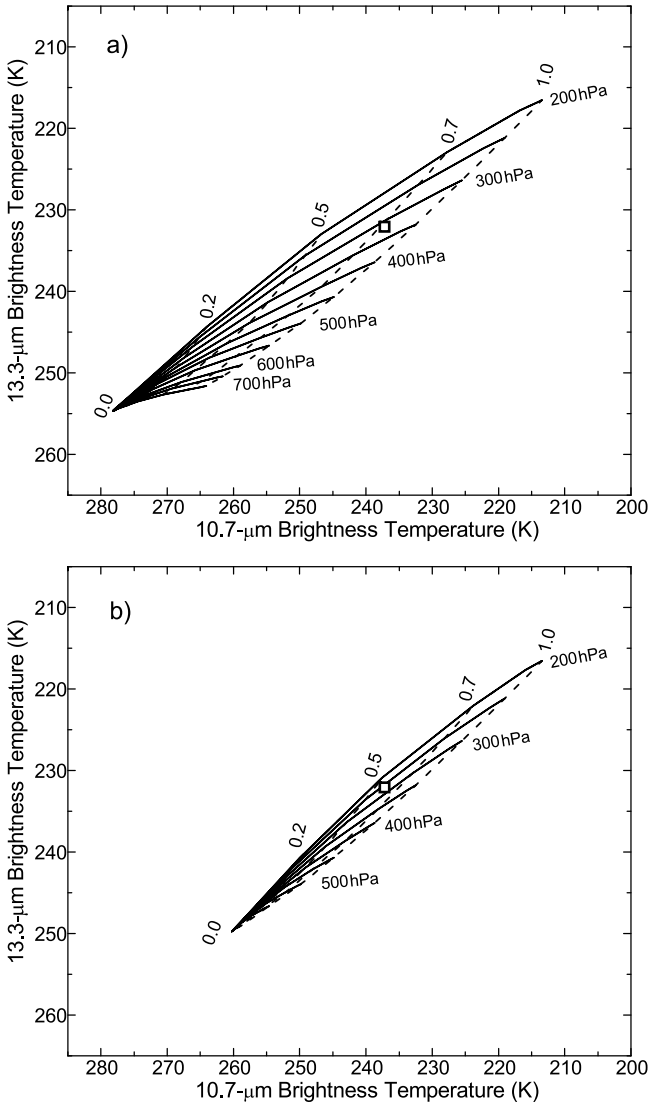

Figure 2. The 10.7 and 13.3 μm brightness temperatures for clouds at different P_c (solid lines) and different ε_c^{11} (dashed lines) for the ARM SGP site at 1045 UTC, 1 May 2005. (a) Calculations from the SCO2AT. (b) Calculations from the MCO2AT. The GOES 12 pixel 10.7 and 13.3 μm brightness temperatures are marked by the square.

uncertainties of the surface and atmospheric temperature profile. If the SCO2AT-inferred $P_c < 600$ hPa, the retrieval will proceed to the second step to compare the satellite-observed R_{obs}^{13} with an initial estimate of $R_{ebg}^{13} - \delta_R^{13}$, where the threshold $\delta_R^{13} = 0.1$ Wm^{-2}sr$^{-1}\mu$m^{-1} is used to account for about five times the instrument noise level of the GOES 12 imager 13.3 μm radiance observations. If R_{obs}^{13} is not less than the initial estimate, the retrieval will stop and the solution is assigned with the SCO2AT-inferred P_c. If R_{obs}^{13} is less than $R_{ebg}^{13} - \delta_R^{13}$, the retrieval will proceed to the third step for an iteration of the MCO2AT.

[20] More details for step 2 are given by 2A-2D and for step 3 are given by 3A-3G as listed here:

2A. Set initial R_{ebg}^{11} ($T_{ebg}|P_{ebg}$) to equal R_{obs}^{11}.

2B. Use the initial R_{ebg}^{11} and equation (9) to retrieve an initial estimate of $T_{ebg}|P_{ebg}$.

2C. Use equation (10) to infer an initial estimate of R_{ebg}^{13} ($T_{ebg}|P_{ebg}$).

2D. Compare the satellite-observed R_{obs}^{13} with the initial R_{ebg}^{13}. If $R_{obs}^{13} < R_{ebg}^{13} - \delta_R^{13}$, proceed to 3A-3G.

3A. Infer a new 13.3 μm effective emissivity ε_c^{13} by

$$\varepsilon_c^{13} = \frac{R_{obs}^{13} - R_{ebg}^{13}(T_{ebg}|P_{ebg}))}{(R_{ovc}^{13}(T_c|P_c) - R_{ebg}^{13}(T_{ebg}|P_{ebg}))}. \quad (13)$$

3B. Use equation (11) and the new ε_c^{13} to infer a new ε_c^{11}.

3C. Infer a new 10.7 μm effective background radiance R_{ebg}^{11} by

$$R_{ebg}^{11}(T_{ebg}|P_{ebg}) = \frac{R_{obs}^{11} - \varepsilon_c^{11} R_{ovc}^{11}(T_c|P_c)}{(1 - \varepsilon_c^{11})}, \quad (14)$$

but constrain the new R_{ebg}^{11} by a maximum at $R_{ebg}^{11} = R_{clr}^{11}$ and a minimum at $R_{ebg}^{11} = (R_{clr}^{11} + R_{obs}^{11})/2$.

3D. Use equation (9) and the new R_{ebg}^{11} to retrieve new $T_{ebg}|P_{ebg}$.

3E. Use equation (10) and the new $T_{ebg}|P_{ebg}$ to infer a new R_{ebg}^{13}.

3F. Use equation (8) and the new $T_{ebg}|P_{ebg}$ to retrieve new $T_c|P_c$.

3G. If |new R_{ebg}^{13} − old R_{ebg}^{13} | > δ_R^{Ch6}, repeat 3A–3G.

[21] The above retrieval algorithm will give a cloud pixel a possible upper CTH solution set $[P_c, T_c]$ inferred by the MCO2AT for an enhanced CO_2-CTH or by the SCO2AT for a regular CO_2-CTH. The upper CTH is inferred by finding the altitude corresponding to P_c using the RUC vertical profile of pressure levels. The threshold of 600 hPa (~4.3 km) is selected conservatively because the CO_2 absorption technique is based on the well-mixed nature of CO_2 in the upper troposphere and the CO_2-CTH becomes less certain in the lower troposphere due to its reduced signal-to-noise ratio. There may be a possible low-level CTH solution, which would require the window technique and/or a more robust cloud retrieval algorithm, but that is beyond the scope of this study. In this paper, we only focus on the results derived from the SCO2AT and MCO2AT.

[22] Figure 2 shows an example of the 10.7 and 13.3 μm brightness temperatures calculated from the SCO2AT (Figure 2a) and MCO2AT (Figure 2b) for clouds at different pressure levels (solid lines) and different ε_c^{11} (dashed lines). The calculations are for the atmospheric profiles obtained at the ARM SGP site at 1045 UTC on 1 May 2005. The ground surface temperature T_g is 283 K for the SCO2AT in Figure 2a and the inferred effective background temperature T_{ebg} is 262.5 K for the MCO2AT in Figure 2b. The collocated GOES 12 imager pixel has the observed 10.7 and 13.3 μm brightness temperatures of 237.3 K and 232.1 K, respectively. The cloud in the imager pixel is clearly not an opaque cloud since the SCO2AT-inferred ε_c^{11} is about 0.7 (Figure 2a) and the MCO2AT-inferred ε_c^{11} is about 0.57 (Figure 2b). The SCO2AT-inferred P_c is about 315 hPa (Figure 2a), which is enhanced to $P_c \sim 265$ hPa by the MCO2AT (Figure 2b).

[23] Because it solves explicitly for T_{ebg}, the MCO2AT is applicable to both single-layer and multilayer cloud pixels and works more effectively for transmissive cirrus clouds in multilayer situations or geometrically thick, tenuous clouds.

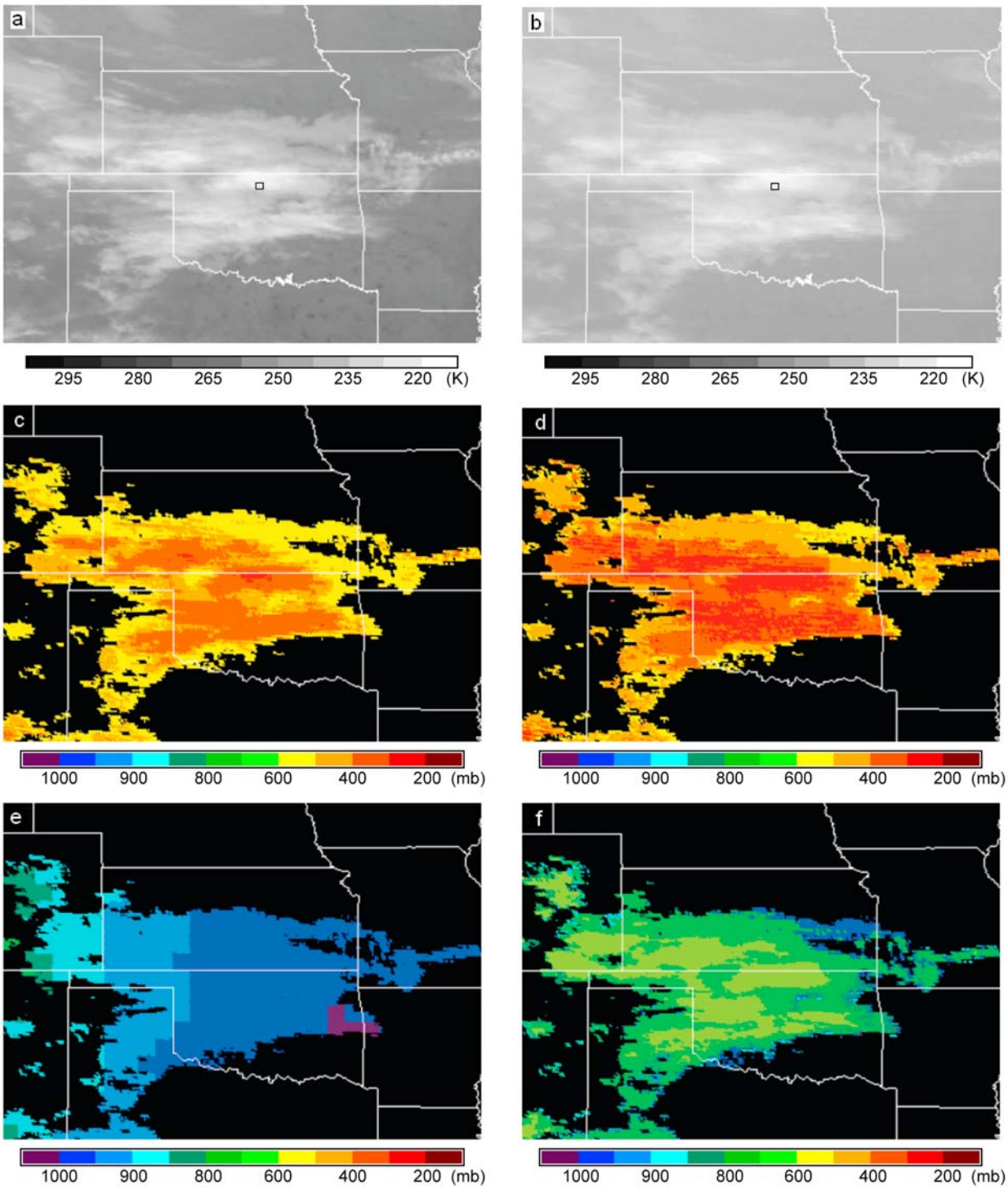

Figure 3. GOES 12 images of the (a) 10.7 μm and (b) 13.3 μm channel brightness temperatures, the associated SCO2AT (c) P_c and (e) P_g, and the associated MCO2AT (d) P_c and (f) P_{ebg} for an area of 32°N–42°N and 105°W–91°W at 1045 UTC, 1 May 2005. The squares in Figures 3a and 3b indicate the ARM SGP CART site.

For the cirrus-overlying-stratus cloud situation, the effective background level is higher than the ground level (i.e., $P_{ebg} < P_g$) and the MCO2AT-inferred CTH will be raised higher than the SCO2AT-inferred CTH. For the geometrically thick, tenuous cloud situation, the effective background level is also higher than the ground level and likewise the MCO2AT-inferred CTH will be also higher than the SCO2AT-inferred CTH. For the situations having more opaque upper troposphere clouds, the MCO2AT-inferred CTH would only be slightly higher than the SCO2AT-in-

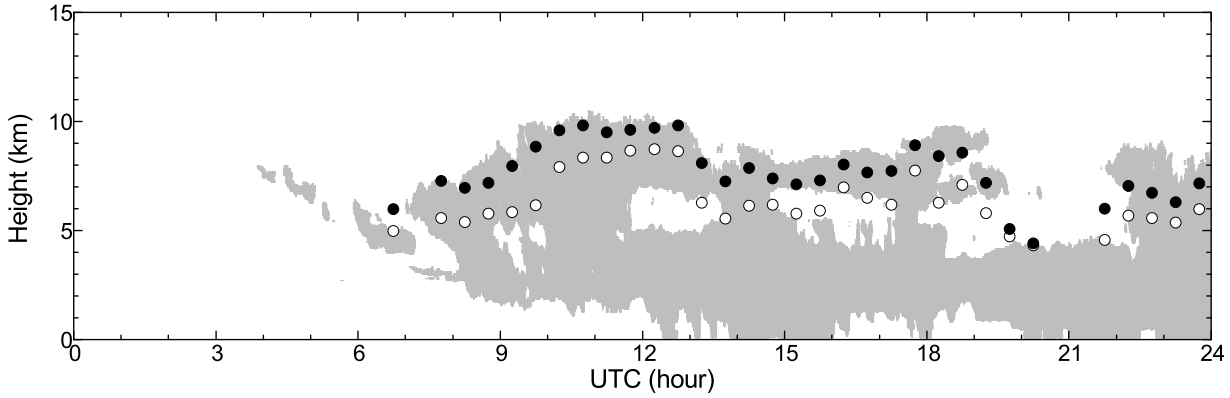

Figure 4. Comparisons between the MCO2AT (solid circles) and SCO2AT (open circles) mean Z_c and the ARSCL vertical profile over the ARM SGP site on 1 May 2005.

ferred CTH, even though the MCO2AT-inferred effective background level will be higher than the ground level. This is because the upper-level opaque CTHs inferred by both MCO2AT and SCO2AT are less sensitive to the different effective background radiances. This can be seen in Figures 2a and 2b where the dashed lines with $\varepsilon_c^{11} = 1$ are nearly identical for $P_c < 500$ hPa. Thus, the more opaque the upper cloud, the smaller the difference between the SCO2AT- and MCO2AT-inferred CTHs. Moreover, as described earlier in step 3C, the MCO2AT-inferred 10.7 μm effective background radiance R_{ebg}^{11} is constrained by a midway threshold between the clear-sky and satellite-observed 11 μm radiances, i.e., $(R_{clr}^{11} + R_{obs}^{11})/2$. As a result, the effective background temperature T_{ebg} inferred by the MCO2AT is always bound by the clear-sky temperature and the satellite-observed 11 μm brightness temperature.

4. Comparisons

4.1. Comparisons With ARSCL Data

[24] Figure 3 demonstrates the SCO2AT- and MCO2AT-inferred CTPs using GOES 12 10.7 μm (Figure 3a) and 13.3 μm (Figure 3b) brightness temperatures obtained at 1045 UTC on 1 May 2005 over the SGP domain that extends from 32°N to 42°N and from 105°W to 91°W. The ARM SGP CART site is indicated by the little square near the center of the images. The 13.3 μm brightness temperatures in Figure 3b are obscured by the CO_2 absorption and thus appear colder (brighter) than the 10.7 μm brightness temperatures in Figure 3a. Figures 3c–3f show the corresponding values of the SCO2AT P_c and P_g and the MCO2AT P_c and P_{ebg}. The MCO2AT P_c values are generally smaller (higher in altitude) than the SCO2AT P_c and their mean difference is about 70 hPa. Similarly, the MCO2AT P_{ebg} values are generally smaller than P_g and their mean difference is about 240 hPa. There are 48 such half-hourly GOES 12 images analyzed on each day of May 2005, so a total of 1488 cases are analyzed. A spatial average of z_c is obtained within a 15 km × 15 km area centered at the SGP CART site. If all the GOES 12 imager pixels within the 15 km area have valid P_c retrievals, it is considered as a completely overcast upper cloud scene. If only part of the imager pixels within the 15 km area have valid P_c retrieval, it is classified as a broken upper cloud scene.

[25] In order to compare with the ARSCL CTH data, the MCO2AT- and SCO2AT-retrieved pixel-scale P_c are first converted to $z_c(P_c)$ using the RUC vertical profiles of height and pressure levels. Second, from each half-hourly GOES 12

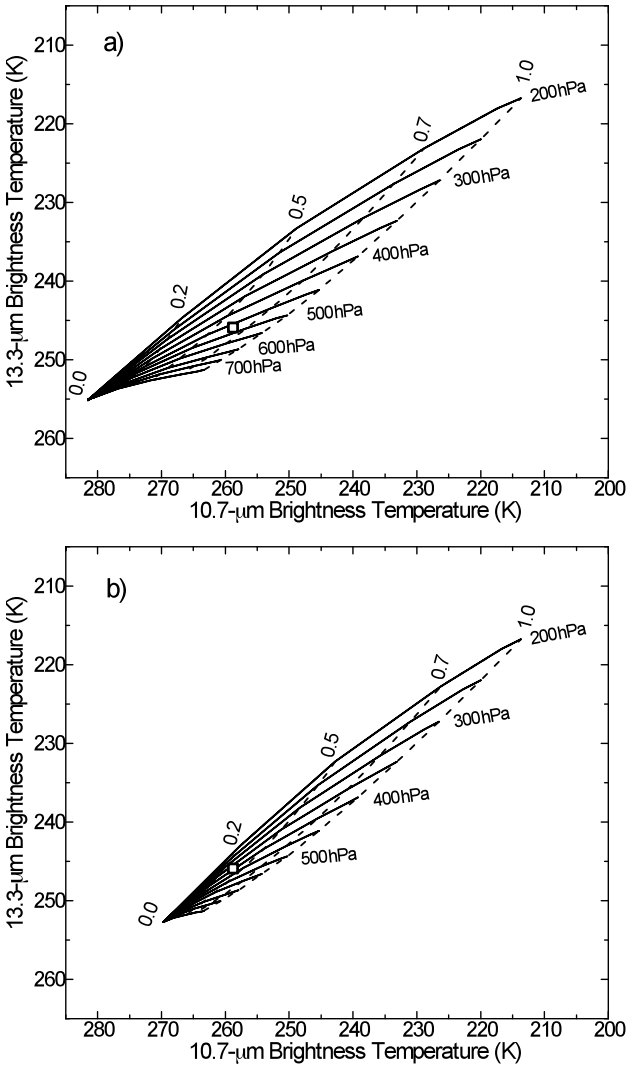

Figure 5. Same as in Figure 2 but for the data obtained at 1545 UTC.

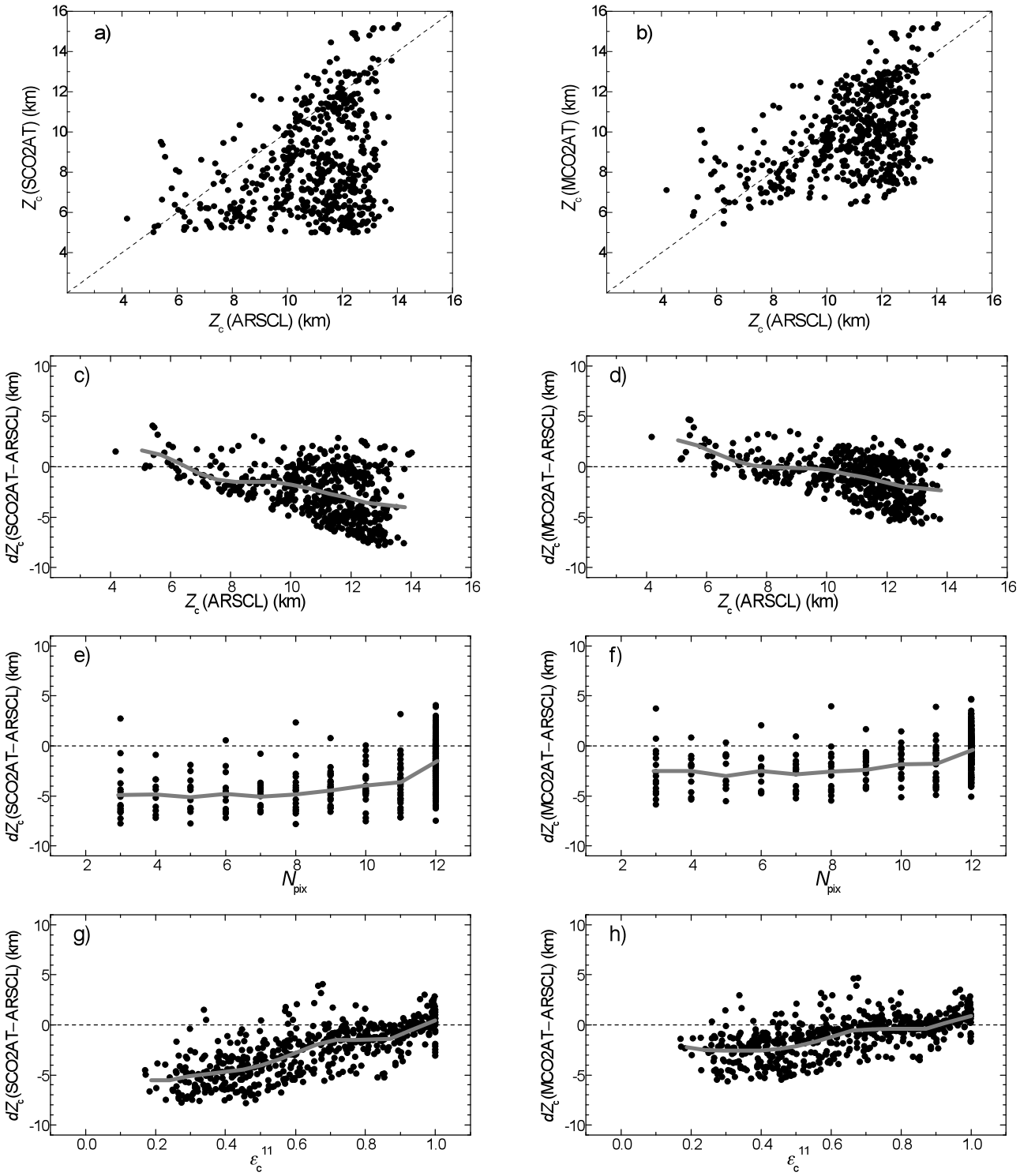

Figure 6. (a) Mean Z_c (SCO2AT) versus mean Z_c (ARSCL). (b) Mean Z_c (MCO2AT) versus mean Z_c (ARSCL). (c) Mean difference dZ_c (SCO2AT − ARSCL) versus Z_c (ARSCL). (d) Mean difference dZ_c (MCO2AT − ARSCL) versus Z_c (ARSCL). (e) Mean difference dZ_c (SCO2AT − ARSCL) versus N_{pix}. (f) Mean difference dZ_c (MCO2AT − ARSCL) versus N_{pix}. (g) Mean difference dZ_c (SCO2AT − ARSCL) versus ε_c^{11}. (h) Mean difference dZ_c (MCO2AT − ARSCL) versus ε_c^{11}. Grey thick lines are for the running means.

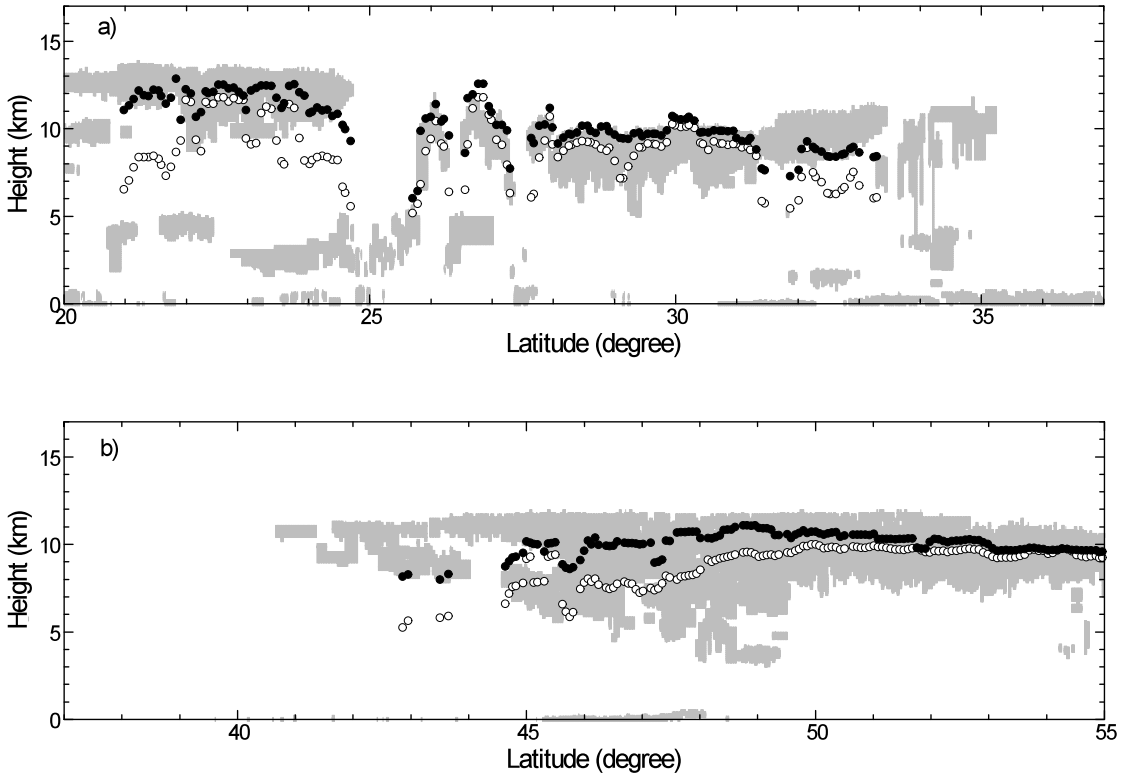

Figure 7. Comparisons between the MCO2AT-inferred (solid circles) and SCO2AT-inferred (open circles) mean Z_c and the CALIOP (light gray) vertical cloud mask for (a) 0745 UTC 10 April 2007 and (b) 1745 UTC 22 April 2007.

analysis, a spatial average of z_c was computed for the 15 km area centered at the SGP CART site. Figure 4 shows the half-hourly mean z_c from the MCO2AT (solid circle) and SCO2AT (open circle) obtained on 1 May 2005, along with the time series of the ARSCL cloud vertical profile plotted in gray. The differences between the MCO2AT- and SCO2AT-inferred mean z_c are approximately 1–2 km on this day, where the MCO2AT mean z_c are generally in better agreement with the ARSCL uppermost CTHs than the SCO2AT mean z_c.

[26] Figure 5 shows another example of the 10.7 and 13.3 μm brightness temperatures calculated from the SCO2AT (Figure 5a) and MCO2AT (Figure 5b) for clouds at different pressure levels (solid lines) and with different ε_c^{11} (dashed lines). This example is for a multilayered cloud pixel having the brightness temperatures of about 259 K (10.7 μm) and 246 K (13.3 μm) obtained at 1545 UTC on 1 May 2005 (see Figure 4). The upper layer cloud in this case is semi-transparent (small emissivity), resulting in underestimation of the upper CTH. The MCO2AT P_c is decreased by about 60 hPa and the MCO2AT CTH is above 1.5 km higher than the SCO2AT-inferred CTH.

[27] To evaluate the performance of the MCO2AT relative to the SCO2AT, the ARSCL uppermost CTH data obtained within ±1.5 min of the GOES 12 scan time at the SGP CART site were used to calculate a mean ARSCL z_c for comparison with the 15 km means from the two satellite methods. Of the 1488 cases, 25% were found having completely overcast upper cloud scenes in the 15 km areas. About 18% of the cases were found to be broken upper cloud scenes, which had some pixels without a z_c retrieval. More than 10% of the cases had no valid z_c retrieval in the 15 km area, but the ARSCL data had upper-level clouds. These cases appeared to be optically thin clouds and were not compared in this study. The broken upper cloud scenes used in this study were limited to those having more than two pixels having valid P_c retrievals. Those having only one or two pixel P_c retrievals were not compared.

[28] Figure 6 shows the comparisons of the mean z_c between the ARSCL and the SCO2AT (Figure 6, left) and MCO2AT (Figure 6, right) from all overcast and broken upper cloud scenes as functions of different variables. Figures 6a and 6b show scatterplots of the SCO2AT and the MCO2AT CTHs, respectively, versus ARSCL z_c. The overall mean (±standard deviations) are 10.95 (±1.82) km for the ARSCL, 8.42 (±2.48) km for the SCO2AT, and 9.94 (±1.97) km for the MCO2AT. The mean z_c is ~1 km smaller for MCO2AT and ~2.5 km smaller for SCO2AT than for ARSCL. The MCO2AT raised the SCO2AT mean z_c by 1.5 km. However, Figures 6a and 6b also show larger differences from individual cases with both overestimation and underestimation. The differences may be due to data mismatches from the two different satellite and ground-based observation platforms and/or due to other factors as further evaluated in Figures 6c–6h.

[29] Figures 6c and 6d show the differences dz_c in z_c between the SCO2AT and ARSCL and between the MCO2AT and ARSCL, respectively, as a function of the ARSCL z_c. Both SCO2AT and MCO2AT overestimate z_c more often at lower ARSCL z_c and underestimate z_c more frequently at

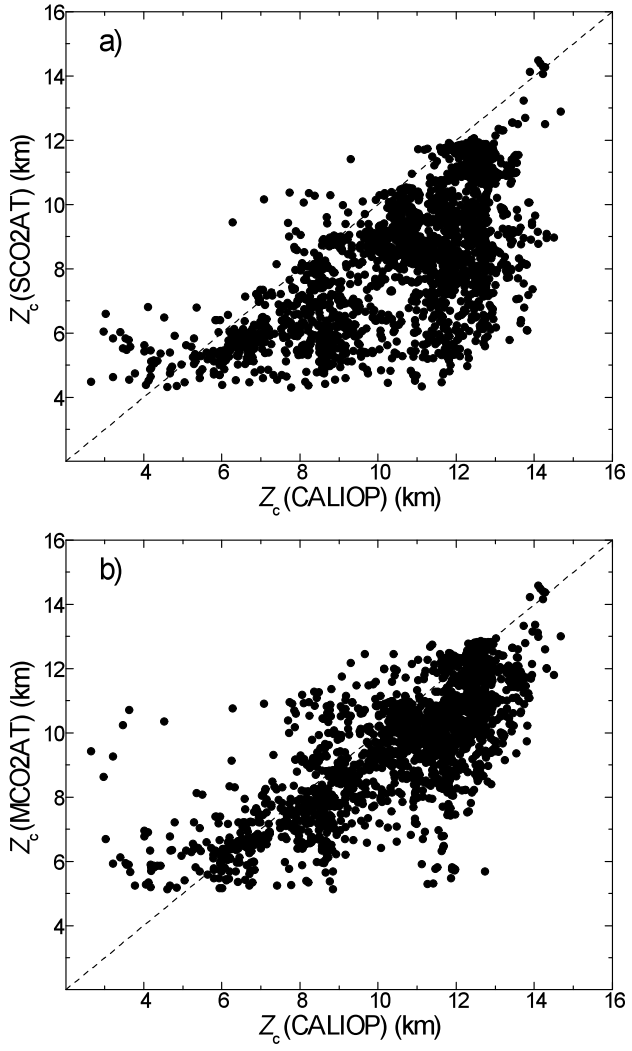

Figure 8. Comparisons for (a) SCO2AT Z_c versus CALIOP Z_c and (b) MCO2AT Z_c versus CALIOP Z_c.

higher ARSCL z_c. The overestimation may be due to the GOES 12 imager viewing a larger cloud volume with higher CTHs nearby that were not seen by the ARSCL radar/lidar vertical-pointing view or that the SCO2AT and MCO2AT had overestimated some of the upper CTHs, while underestimating many more cases. For thicker ice clouds, the surface radar/lidar combination is often unable to detect the cloud tops [e.g., *Mace and Benson,* 2008]. Thus, the satellite could easily appear to overestimate CTH in those cases.

[30] Figures 6e and 6f plot dz_c (SCO2AT − ARSCL) and dz_c (MCO2AT − ARSCL), respectively, as a function of N_{pix}, the number of GOES 12 imager pixels having valid z_c retrieval in the 15 km area. Only the cases with N_{pix} = 3–12 are analyzed, where N_{pix} = 12 are from those cases having a completely overcast upper cloud scene and N_{pix} = 3–11 are from those cases having a broken upper cloud scene. Those cases having an overcast upper cloud scene had better agreement with the ARSCL z_c than cases with a broken upper cloud scene. For all cases of N_{pix} = 12, the mean dz_c (SCO2AT − ARSCL) and dz_c (MCO2AT − ARSCL) are −1.6 (±2.1) km and −0.3 (±1.5) km, respectively. It is also noted that both the absolute mean dz_c (SCO2AT − ARSCL) and dz_c (MCO2AT − ARSCL) increase significantly from N_{pix} = 12 to N_{pix} = 11 and then increase gradually toward smaller N_{pix}. It appears that even one broken pixel can make a large difference, possibly due to thinner clouds near cloud edges. For all broken upper cloud scenes having N_{pix} between 3 and 11, the mean dz_c (SCO2AT − ARSCL) and dz_c (MCO2AT − ARSCL) are −4.7 (±2.3) km and −2.7 (±1.8) km, respectively. These biases are much larger than those for the overcast upper cloud scenes.

[31] In Figures 6g and 6h, dz_c (SCO2AT − ARSCL) and dz_c (MCO2AT − ARSCL) are plotted against the MCO2AT-inferred ε_c^{11}. The absolute mean differences and standard deviations both increase with decreasing ε_c^{11}. The results show more increases in $|dz_c|$ with decreasing ε_c^{11} for the SCO2AT than for the MCO2AT, which indicate that the CTH errors are reduced at all cloud optical depths from the new method compared to the SCO2AT. The slight overestimate for ε_c^{11} near 1.0 is consistent with the underestimation of CTH by the surface radar/lidar complement for optically thick ice clouds.

4.2. Comparisons With CALIOP Data

[32] The half-hourly GOES 12 imagery data were matched with the CALIOP data over the CONUS and western North Atlantic Ocean between 20°N and 55°N during the month of April 2007. The region selection is partly due to the limited spatial domain of the RUC reanalysis data. The comparisons are limited to only the GOES 12 imagery data obtained during 1, 4, 7, 10, 13, 16, 19, 22, 25 and 28 April and with satellite viewing zenith angles less than 65°. The maximum time difference in the matched data is limited to ±10 min between the GOES 12 and CALIOP observations.

[33] Figure 7 illustrates the SCO2AT- and MCO2AT-inferred CTHs matched with two sections of the CALIOP vertical cloud mask taken at ~0745 UTC, 10 April 2007 and at ~1745 UTC, 22 April 2007. The mean z_c in the demonstrated examples from SCO2AT and MCO2AT, respectively, are 8.68 (±1.69) km and 10.32 (±1.45) km (MCO2AT) for Figure 7a and 8.89 (±1.11) km and 10.06 (±0.62) km for Figure 7b. Note that some of the CALIOP-observed upper-level clouds were missed by the SCO2AT and MCO2AT. In Figure 7a, no matched data were obtained outside of 21°N and 33.5°N latitudes.

[34] The matched values of z_c between CALIOP and the SCO2AT and MCO2AT retrievals for more than 3000 matched cases are plotted in Figures 8a and 8b, respectively. The CALIOP mean z_c was obtained by averaging the detected uppermost CTHs within the 3 × 3 imager pixel array. The SCO2AT and MCO2AT mean z_c were obtained by averaging the valid z_c retrievals, where at least 3 out of 9 pixels with valid z_c are included in the comparisons. The overall z_c averages for the CALIOP, SCO2AT, and MCO2AT are 10.75 (±2.13), 8.35 (±2.07) and 9.73 (±1.84) km, respectively. The mean z_c is ~1 km smaller for MCO2AT and ~2.4 km smaller for SCO2AT than for CALIOP, where some individual cases show larger positive and negative differences. The MCO2AT is greater than the SCO2AT mean z_c by about 1.4 km, which is similar to ~1.5 km obtained earlier over the ARM SGP site.

[35] Following the approach used for Figure 6, the differences between the CALIOP, SCO2AT and MCO2AT are plotted as functions of the possible factors that could cause

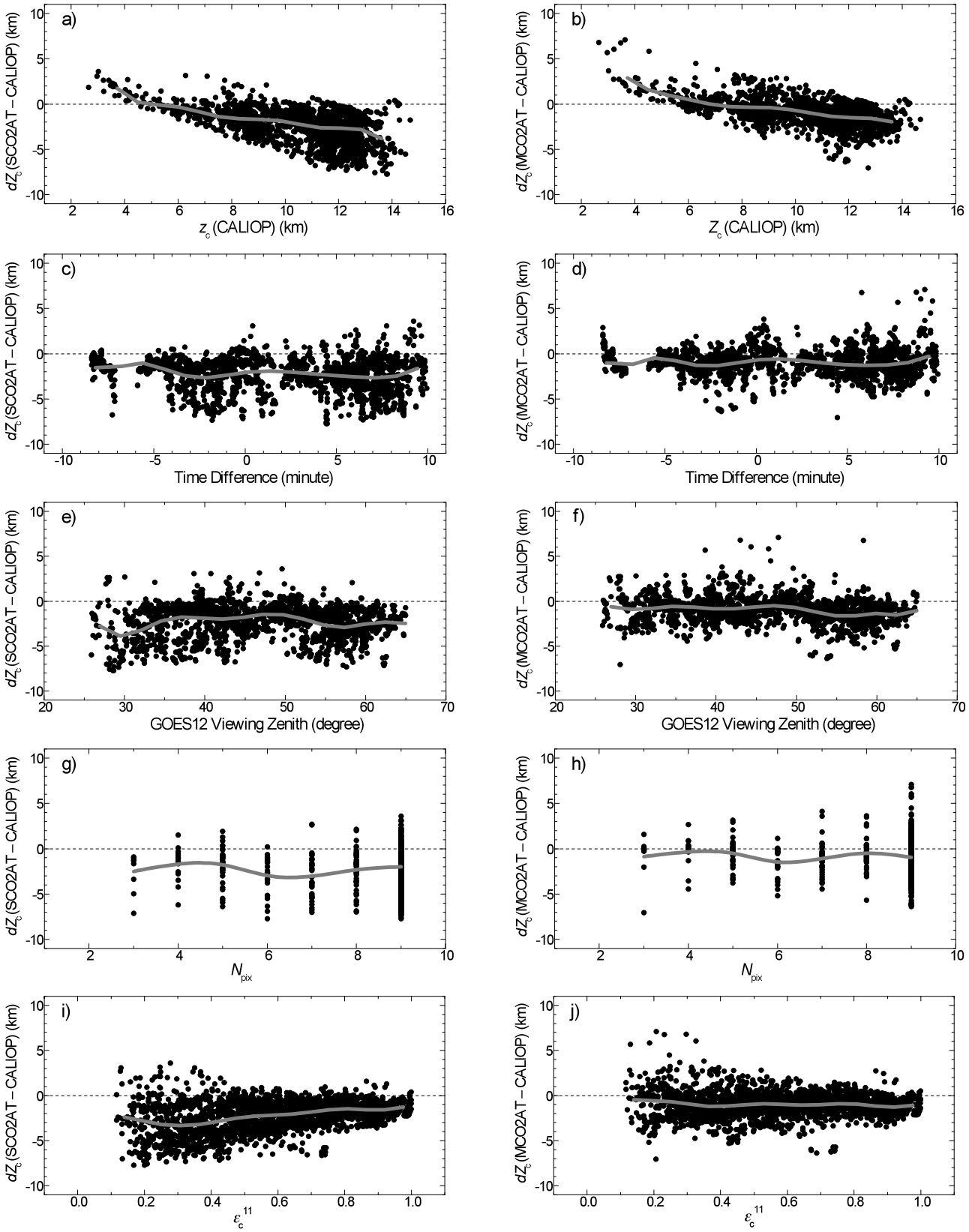

Figure 9. (a, c, e, g, i) The mean difference dZ_c (SCO2AT minus CALIOP) and (b, d, f, h, j) the mean difference dZ_c (MCO2AT minus CALIOP) as a function of the CALIOP Z_c (Figures 9a and 9b), the time difference between CALIOP and GOES 12 (Figures 9c and 9d), the GOES 12 viewing zenith (Figures 9e and 9f), the N_{pix} (Figures 9g and 9h), and ε_c^{11} (Figures 9i and 9j). Grey thick lines are for the running means.

large individual differences. In general, both the SCO2AT and MCO2AT tend to overestimate z_c more at lower z_c and underestimate z_c more often at higher z_c (Figures 9a and 9b) as seen earlier (Figures 6c and 6d). There appears to be negligible dependence of dz_c on the time differences (Figures 9c and 9d), at least, for the window used here. Likewise, there is no strong variation of dz_c with viewing zenith angle (Figures 9e and 9f) despite the potential for large parallax errors. Unlike the results in Figures 6e and 6f, dz_c appears to have no strong dependence on N_{pix} in Figures 9g and 9h. Last, in Figure 9i, dz_c (SCO2AT) varies systematically with ε_c^{11} as seen in Figure 6g. Contrary to the results in Figure 6h, however, there is no indication of such dependence for MCO2AT in Figure 9j where the mean biases are nearly the same (~1 km) for the entire emissivity range. In Figures 9i and 9j, there are few overestimates of CTH for optically thick clouds ($\varepsilon_c^{11} \sim 1.0$) whereas in Figures 6g and 6h, there are more overestimates of CTH for the optically thick clouds. This may indicate the underestimates of the top heights of these clouds from the surface-based radar.

5. Concluding Remarks

[36] Accurate inferences of upper troposphere cloud top heights (CTHs) for geometrically thick but optically thin clouds are often difficult using passive meteorological satellite observations. For transmissive upper-level clouds, the inferences become more difficult in multilayer cloud situations when lower clouds coexist underneath the upper clouds. Operational meteorological satellite analyses have shown much success in using the CO_2 absorption techniques to retrieve the CTH information for transmissive cirrus clouds, but all current retrieval methods are based on single-layer cloud assumptions. They commonly assume that the cloud layer occupies an infinitesimal thickness in vertical extent and that underneath the geometrically thin cloud layer is a cloud-free atmosphere over the surface. The single-layer assumptions may induce large uncertainties in the satellite-inferred CTHs because cloud vertical profiles, as revealed by the data obtained from the cloud radar and lidar, are often complex and a geometrically thin single-layer cloud is relatively infrequent.

[37] To overcome the difficulties with conventional single-layer assumptions, a new a modified CO_2 absorption technique (MCO2AT) for inferring the upper CTH has been presented in this paper. This new method is developed based on a traditional single-layer CO_2 absorption technique (SCO2AT) followed by an iterative retrieval procedure to obtain an enhanced upper CTH for transmissive upper tropospheric clouds. The new method and the traditional SCO2AT are both applied to the 10.7 and 13.3 μm channel data from the GOES 12 imager. Comparisons of the two upper CTHs inferred from the GOES 12 data show average increases of ~1.5 km by the MCO2AT relative to the SCO2AT. When they are compared to the ARM ARSCL products derived from the ground-based radar/lidar data and to the satellite-based CALIOP lidar data over midlatitude regions, the mean CTHs for the MCO2AT and SCO2AT are lower by ~1 km and ~2.5 km, respectively. These comparisons have demonstrated that the MCO2AT is more effective than the SCO2AT for inferring upper tropospheric CTHs for transmissive clouds and the overall inferences of the upper tropospheric CTHs from the MCO2AT are closer to the physical cloud tops detected by the surface and satellite-based active instruments.

[38] The new modified method, which uses only 10.7 and 13.3 μm data, is particularly useful for passive sensors like the GOES 12, 13 and beyond, because those sensors carry five channels, but only the two 10.7 and 13.3 μm thermal IR channels are available for inferring upper tropospheric CTH. The modified method is applicable to data from instruments on other satellites having similar spectral bands. These would include the currently operating Spinning Enhanced Visible and Infrared Imager (SEVIRI) onboard Meteosat-8 and -9 and the MODIS on Terra and Aqua, as well as on upcoming satellites such as GOES-R. Future work includes applications to other satellite data and additional comparisons with surface and space-based active remote sensing measurements to determine the accuracy of the new method over a wide range of cloud, surface, and weather conditions.

[39] **Acknowledgments.** This research has been supported by the NASA Advanced Satellite Aviation-weather Products initiative, the NASA Applied Sciences Program, the Department of Energy ARM Program through DE-AI02-07ER64546, and the NOAA Center for Satellite Applications and Research GOES-R Program.

References

Ackerman, T. P., and G. Stokes (2003), The Atmospheric Radiation Measurement Program, *Phys. Today*, *56*, 38–45, doi:10.1063/1.1554135.

Ayers, J. K., et al. (2006), Overview of NASA Langley ARM cloud products and validation, paper presented at Sixteenth ARM Science Team Meeting, U.S. Dep. of Energy, Washington, D. C. (Available at http://www.arm.gov/publications/proceedings/conf16/extended_abs/ayers_jk.pdf)

Bedka, S. T., W. F. Feltz, A. J. Schreiner, and R. E. Holz (2007), Satellite-derived cloud top pressure product validation using aircraft-based cloud physics lidar data from the ATReC field campaign, *Int. J. Remote Sens.*, *28*, 2221–2239, doi:10.1080/01431160500391965.

Benjamin, S. G., G. A. Grell, J. M. Brown, T. G. Smirnova, and R. Bleck (2004a), Mesoscale weather prediction with the RUC hybrid isentropic-terrain-following coordinate model, *Mon. Weather Rev.*, *132*, 473–494, doi:10.1175/1520-0493(2004)132<0473:MWPWTR>2.0.CO;2.

Benjamin, S. G. et al. (2004b), An hourly assimilation-forecast cycle: The RUC, *Mon. Weather Rev.*, *132*, 495–518, doi:10.1175/1520-0493(2004)132<0495:AHACTR>2.0.CO;2.

Berk, A., et al. (1999), MODTRAN4 v. 2.0 user's manual, *Tech. Rep. AFGL-TR-89-0122*, 98 pp., Air Force Geophys. Lab., Air Force Mat. Comm., Hanscomb AFB, Mass.

Chahine, M. T. (1974), Remote sounding of cloudy atmospheres. I. The single cloud layer, *J. Atmos. Sci.*, *31*, 233–243, doi:10.1175/1520-0469(1974)031<0233:RSOCAI>2.0.CO;2.

Chang, F.-L., and Z. Li (2005), A near-global climatology of single-layer and overlapped clouds and their optical properties retrieved from Terra/MODIS data using a new algorithm, *J. Clim.*, *18*, 4752–4771, doi:10.1175/JCLI3553.1.

Clothiaux, E. E., T. P. Ackerman, G. G. Mace, K. P. Moran, R. T. Marchand, M. Miller, and B. E. Martner (2000), Objective determination of cloud heights and radar reflectivities using a combination of active remote sensors at the ARM CART sites, *J. Appl. Meteorol.*, *39*, 645–665, doi:10.1175/1520-0450(2000)039<0645:ODOCHA>2.0.CO;2.

Eyre, J. R., and W. P. Menzel (1989), Retrieval of cloud parameters from satellite sounder data: A simulation study, *J. Appl. Meteorol.*, *28*, 267–275, doi:10.1175/1520-0450(1989)028<0267:ROCPFS>2.0.CO;2.

Frey, R. A., B. A. Baum, W. P. Menzel, S. A. Ackerman, C. C. Moeller, and J. D. Spinhirne (1999), A comparison of cloud top heights computed from airborne lidar and MAS radiance data using CO_2 slicing, *J. Geophys. Res.*, *104*, 24,547–24,555, doi:10.1029/1999JD900796.

Hawkinson, J. A., W. F. Feltz, and S. A. Ackerman (2005), A comparison of GOES sounder and cloud lidar- and radar-retrieved cloud-top heights, *J. Appl. Meteorol.*, *44*, 1234–1242, doi:10.1175/JAM2269.1.

Holz, R. E., S. Ackerman, P. Antonelli, F. Nagle, R. O. Knuteson, M. McGill, D. L. Hlavka, and W. D. Hart (2006), An improvement to

the high-spectral-resolution CO2-slicing cloud-top altitude retrieval, *J. Atmos. Oceanic Technol.*, *23*, 653–670, doi:10.1175/JTECH1877.1.

Jin, Y., W. B. Rossow, and D. P. Wylie (1996), Comparison of the climatologies of high-level clouds from HIRS and ISCCP, *J. Clim.*, *9*, 2850–2879, doi:10.1175/1520-0442(1996)009<2850:COTCOH>2.0.CO;2.

Mace, G. G., and S. M. Benson (2008), The representativeness of ARM cloud measurements: Initial comparison of ARM cloud statistics with CloudSat and CALIPSO statistics, paper presented at 18th Annual ARM Science Team Meeting., Norfolk, Va., 10–14 March. (Available at http://www.arm.gov/publications/proceedings/conf18/poster/P00170.pdf).

McCleese, D. J., and L. S. Wilson (1976), Cloud top heights from temperature sounding instruments, *Q. J. R. Meteorol. Soc.*, *102*, 781–790, doi:10.1002/qj.49710243408.

Menzel, W. P., and J. F. W. Purdom (1994), Introducing GOES-I: The first of a new generation of geostationary operational environmental satellites, *Bull. Am. Meteorol. Soc.*, *75*, 757–781, doi:10.1175/1520-0477(1994)075<0757:IGITFO>2.0.CO;2.

Menzel, W. P., W. L. Smith, and T. R. Stewart (1983), Improved cloud motion vector and altitude assignment using VAS, *J. Clim. Appl. Meteorol.*, *22*, 377–384, doi:10.1175/1520-0450(1983)022<0377:ICMWVA>2.0.CO;2.

Menzel, W. P., D. P. Wylie, and K. I. Strabala (1992), Seasonal and diurnal changes in cirrus clouds as seen in four years of observations with the VAS, *J. Appl. Meteorol.*, *31*, 370–385, doi:10.1175/1520-0450(1992)031<0370:SADCIC>2.0.CO;2.

Minnis, P., K.-N. Liou, and Y. Takano (1993), Inference of cirrus cloud properties using satellite-observed visible and infrared radiances. Part I: Parameterization of radiance field, *J. Atmos. Sci.*, *50*, 1279–1304, doi:10.1175/1520-0469(1993)050<1279:IOCCPU>2.0.CO;2.

Minnis, P., C. R. Yost, S. Sun-Mack, and Y. Chen (2008), Estimating the physical top altitude of optically thick ice clouds from thermal infrared satellite observations using CALIPSO data, *Geophys. Res. Lett.*, *35*, L12801, doi:10.1029/2008GL033947.

Rossow, W. B. (1989), Measuring cloud properties from space: A review, *J. Clim.*, *2*, 201–213, doi:10.1175/1520-0442(1989)002<0201:MCPFSA>2.0.CO;2.

Rossow, W. B., and R. A. Schiffer (1991), ISCCP cloud data products, *Bull. Am. Meteorol. Soc.*, *72*, 2–20, doi:10.1175/1520-0477(1991)072<0002:ICDP>2.0.CO;2.

Schmit, T. J., E. M. Prins, A. J. Schreiner, and J. J. Gurka (2001), Introducing the GOES-M imager, *Natl. Weather Assoc. Digest*, *25*, 28–37.

Schreiner, A. J., T. J. Schmit, and W. P. Menzel (2001), Observations and trends of clouds based on GOES sounder data, *J. Geophys. Res.*, *106*, 20,349–20,363, doi:10.1029/2001JD900213.

Sherwood, S. C., J.-H. Chae, P. Minnis, and M. McGill (2004), Underestimation of deep convective cloud tops by thermal imagery, *Geophys. Res. Lett.*, *31*, L11102, doi:10.1029/2004GL019699.

Smith, W. L., and R. A. Frey (1990), On cloud altitude determinations from high resolution interferometer sounder (HIS) observations, *J. Appl. Meteorol.*, *29*, 658–662, doi:10.1175/1520-0450(1990)029<0658:OCADFH>2.0.CO;2.

Smith, W. L., and C. M. R. Platt (1978), Comparison of satellite-deduced cloud heights with indications from radiosonde and ground-based laser measurements, *J. Appl. Meteorol.*, *17*, 1796–1802, doi:10.1175/1520-0450(1978)017<1796:COSDCH>2.0.CO;2.

Smith, W. L., P. Minnis, H. Finney, R. Palikonda, and M. M. Khaiyer (2008), An evaluation of operational GOES-derived single-layer cloud top heights with ARSCL over the ARM Southern Great Plains site, *Geophys. Res. Lett.*, *35*, L13820, doi:10.1029/2008GL034275.

Wielicki, B. A., and J. A. Coakley Jr. (1981), Cloud retrieval using infrared sounder data: Error analysis, *J. Appl. Meteorol.*, *20*, 157–169, doi:10.1175/1520-0450(1981)020<0157:CRUISD>2.0.CO;2.

Winker, D. M., W. H. Hunt, and M. J. McGill (2007), Initial performance assessment of CALIOP, *Geophys. Res. Lett.*, *34*, L19803, doi:10.1029/2007GL030135.

Wylie, D. P., and W. P. Menzel (1989), Two years of cloud cover statistics using VAS, *J. Clim.*, *2*, 380–392, doi:10.1175/1520-0442(1989)002<0380:TYOCCS>2.0.CO;2.

Yang, P., B.-C. Gao, B. A. Baum, Y. X. Hu, W. J. Wiscombe, S.-C. Tsay, D. M. Winker, and S. L. Nasiri (2001), Radiative properties of cirrus clouds in the infrared (8–13 μm) spectral region, *J. Quant. Spectrosc. Radiat. Transf.*, *70*, 473–504, doi:10.1016/S0022-4073(01)00024-3.

F.-L. Chang, NASA Langley Research Center, Hampton, VA 23681, USA. (fu-lung.chang-1@nasa.gov)

M. M. Khaiyer, R. Palikonda, and D. A. Spangenberg, Science Systems and Applications Inc., 1 Enterprise Pkwy., Suite 200, Hampton, VA 23666, USA.

B. Lin and P. Minnis, NASA Langley Research Center, MS 420, Hampton, VA 23681, USA.